e-ISSN: 2550-164X

Available online at
https://jmeche.uitm.edu.my/browse-journals/special-issues/

Journal of Mechanical Engineering SI 14 2025, 144 – 161.

Journal of Mechanical Engineering

Mechanical Properties of Friction Stir Welded AL 6061-T6: Influence of Welding Parameters and Tool Geometries

Armansyah[1], Sayed Mohamadbagher Tabatabaei[2*], Seyyed Ali Latifi Rostami[3], Fuad Khoshnaw[4], Amin Kolahdooz[4], Ferdyanto[1], Cheng Yee Low[5], Muhammad Afiff Kusumah[1]

[1]*Faculty of Engineering, Universitas Pembangunan Nasional Veteran, Jl. RS. Fatmawati Raya, Pd. Labu, 12450 Jakarta, Indonesia*
[2]*R&D Engineer, BEHnam Pajouh Sepahan Industrial, Iran*
[3]*Aerospace Systems Research Center, Gyeongsang National University, Jinju 52828, Republic of Korea*
[4]*Faculty of Technology, De Montfort University, LE1 9BH Leicester, United Kingdom*
[5]*Faculty of Mechanical and Manufacturing Engineering, Universiti Tun Hussein Onn Malaysia, 86400 Parit Raja, Batu Pahat, Johor, Malaysia*

ARTICLE INFO

Article history:
Received 25 August 2025
Revised 18 October 2025
Accepted 03 November 2025
Online first
Published 15 November 2025

Keywords:
Friction stir welding
Welding parameters
Pins geometry
Residual stresses
Squareness tool

DOI:
10.24191/jmeche.v14i1.8656

ABSTRACT

Achieving strong and defect-free welds in Aluminium alloy 6061-T6 through Friction Stir Welding (FSW) remains a major materials-engineering concern. This research investigated how variations in tool form and key process parameters affect the mechanical response of the welds. Four pin geometries, including cylindrical, conical, square, and threaded-conical, were assessed through controlled experiments involving tensile testing, surface-quality inspection, and residual-stress analysis. Among the tested configurations, the square-pin tool operated at 1250 rpm with a feed rate of 125 mm min^{-1} and a 2° tilt produced the most consistent joint, reaching an ultimate tensile strength of 211.9 MPa (≈ 87 % of the base-metal strength) and a residual stress of 32 MPa within the stir zone. The results also revealed that a zero-degree tilt reduced forging pressure, leading to poor surface finish, and that the relation between feed rate and rotational speed was nonlinear. Strength increased up to an optimum level before declining. The outcomes provided a quantitative basis for selecting FSW parameters that enhanced joint integrity and extended the structural applications of Aluminium alloys.

INTRODUCTION

Age-hardened aluminium alloy 6061-T6 is widely employed in aerospace structures, transportation frames, and power-transmission components because of its favourable combination of strength, weight, formability, and corrosion resistance (Khaleel et al., 2023a; Kolahdooz et al., 2014). Despite these advantages,

[2*] Corresponding author. *E-mail address*: smbtabatabaei@gmail.com
https://doi.org/10.24191/jmeche.v14i1.8656

traditional fusion-based welding often generates defects porosity, hot cracking, and dimensional distortion that degrade mechanical performance.

Friction Stir Welding (FSW) offers a solid-state alternative capable of joining Aluminium and other low-melting-point alloys without melting the base material. The technique, introduced at The Welding Institute (TWI) in 1991 (El-Rayes & El-Danaf, 2012), eliminates recasting and significantly reduces the formation of defects (Maneiah et al., 2020; Newishy et al., 2023). Because weld quality in FSW is governed by both process parameters and tool design, optimizing these factors has become a central theme in current research (Armansyah et al., 2020; Khoshnaw, 2023).

Review of previous research

Numerous investigations have explored how variations in tool design influence the outcome of FSW. Elangovan & Balasubramanian (2008b) observed for alloy AA2219, an 18 mm shoulder diameter produced the most favourable weld formation. Their analysis across fifteen parameter sets showed that a square-pin tool operating at a traverse speed of 0.76 mm s^{-1} resulted in higher tensile strength, greater hardness, and finer grain refinement than other profiles. Likewise, additional work on aluminium 6061 revealed that the combination of a square-pin tool and an 18 mm shoulder consistently led to joints with superior structural quality (Elangovan & Balasubramanian, 2008a).

Further research has emphasised the connection between pin geometry and both the microstructure and the mechanical response of the weld. Ilangovan et al. (2015) reported that threaded pin profiles improved material flow during the joining of dissimilar aluminium alloys (AA6061 and AA5086), producing smaller grain sizes. Baiyao et al. (2020) examined AlLi 2195-T8 subjected to exfoliation-corrosion tests and found that extended exposure (384 h) reduced tensile strength by roughly 13 % and elongation by 17 %. Bahrami et al. (2014) studied the influence of different pin forms in FSW of AA7075 reinforced with SiC nanoparticles. Their results indicated that threaded-conical pins achieved the greatest hardness and most uniform particle dispersion, while cylindrical pins produced the lowest hardness values. Reza-E-Rabby & Reynolds (2014) compared the behaviour of AA6061 and AA7075 during welding, showing that although threaded tools enhance flow and reduce voids, they also raise residual stresses owing to higher local heat generation.

Residual stress itself remains a key concern because it governs the durability and reliability of welded structures. When a component experiences external loads, these residual stresses combine with service stresses and can accelerate failure (Rossini et al., 2012). Techniques used to evaluate residual stress are typically grouped as destructive, semi-destructive, or non-destructive (Khoshnaw, 2023). The first two such as hole drilling, contouring, or sectioning rely on material removal to infer internal stresses, whereas non-destructive approaches employ X-ray diffraction, neutron diffraction, magnetic analysis, or ultrasonic testing (Hutchings et al., 2005).

Buglioni et al. (2015) investigated how travel speed affects longitudinal residual stresses in AA7075 through experimental and numerical work, showing that stress levels rise with increasing speed up to a certain threshold. Richter-Trummer et al. (2012) demonstrated that stronger clamping during FSW of AA2198 minimises distortion and leads to a more uniform residual-stress field. Similarly, Sadeghi et al. (2013) used ultrasonic waves to examine residual stresses in AA5086 and found the highest values along the tool's advancing side. In another study, Moghadam (2015) linked higher rotational speed with elevated residual stresses in AA2024-T351 due to larger thermal gradients, while increased feed rates improved hardness and resistance to plastic deformation.

Identified research gaps

Although extensive studies have been conducted on FSW, several important issues remain insufficiently addressed. First, there is still no comprehensive parametric evaluation that considers the

https://doi.org/10.24191/jmeche.v14i1.8656

combined influence of tool rotation speed, feed rate, and tilt angle on both the mechanical properties and residual stress of aluminium alloy 6061-T6. Many earlier works investigate these parameters independently, leading to incomplete optimization strategies.

Second, only limited attention has been given to achieving a simultaneous balance between low residual stress, high tensile strength, and good surface finish. Most existing analyses focus primarily on improving strength while overlooking the stress distribution that affects long-term performance.

Third, the literature lacks a verified tool geometry that effectively harmonizes material flow, heat generation, and mechanical integrity for Al 6061-T6 under typical manufacturing conditions. Experimental validations that directly connect tool design to stress-reduction mechanisms are particularly scarce. These gaps highlight the need for a controlled and systematic approach to identify the optimal combination of FSW process parameters and tool profiles.

Strategy of the proposed method

To overcome the gaps outlined above, this research adopts a structured experimental methodology designed to explore how FSW process parameters and tool geometries interact to determine joint quality. The program involves a series of controlled trials using four tool shapes: cylindrical, conical, square, and threaded-conical, tested across a matrix of rotational speeds, feed rates, and tilt angles.

Mechanical responses such as ultimate tensile strength, hardness, and surface finish are measured to quantify performance variations. Residual stresses are further assessed using a combination of X-ray diffraction (XRD) and ultrasonic evaluation to map stress distributions throughout the weld zone.

The collected results are statistically analysed to identify parameter combinations that produce the highest joint strength and the lowest residual stresses. The ultimate objective is to establish a validated guideline for selecting FSW process settings that maximize weld quality while ensuring structural reliability in industrial applications

Contributions of the study

This research provides several important advances in understanding FSW of aluminium alloy 6061-T6. The experimental results establish the optimal combination of tool rotation speed, feed rate, and tilt angle that produces the most desirable mechanical characteristics in the welded joints. Through a comparative analysis of four distinct pin geometries, cylindrical, conical, square, and threaded-conical the study clarifies how each design affects heat input, material flow, and microstructural uniformity within the weld zone. In addition, the integration of tensile testing with X-ray diffraction and ultrasonic methods offers a detailed assessment of residual stress behaviour, demonstrating effective ways to minimise internal stresses without reducing joint strength. The data further support the recommendation of a square-pin tool configuration, which enhances material consolidation, limits void formation, and improves the mechanical reliability of the joints. Overall, the findings connect experimental insight with practical application by presenting a validated framework for parameter selection that can be readily applied to industrial processes in aerospace, structural, and manufacturing engineering. By combining mechanical testing, residual-stress evaluation, and process optimisation, this work contributes to both the theoretical understanding and practical refinement of FSW technology.

https://doi.org/10.24191/jmeche.v14i1.8656

MATERIAL AND METHOD

Sample preparation

Sheets of aluminium alloy 6061-T6, each 3 mm thick, served as the base material for the welding experiments. The alloy's chemical composition was verified through spectroscopic analysis conducted with a quantum device at BEHnam Pajouh Sepahan Industrial, and the measured values are reported in Table 1. These findings closely correspond with the standard composition ranges for Al 6061 (T6 temper) given by ASM International and the Aluminium Association in Table 2. The basic mechanical properties of the alloy are summarised in Table 3.

Table 1. Chemical composition of Al6061-T6 Alloy (wt%)

Zn	0.042
Ti	0.023
Si	0.592
Mn	0.043
Mg	1.010
Fe	0.345
Cu	0.259
Cr	0.163
Al	97.400

Table 2. ASM International (Materials Data Handbook) and Aluminum Association (AA 6061 specification)

Element	Standard range (wt%) for Al6061	Result (wt%)
Mg	0.8-1.2	1.01
Si	0.4-0.8	0.592
Fe	$\leq$ 0.7	0.345
Cu	0.15-0.40	0.259
Mn	$\leq$ 0.15	0.0433
Cr	0.04-0.35	0.163
Zn	$\leq$ 0.25	0.0423
Ti	$\leq$ 0.15	0.0225
Al	Balance (~97.5-98.5)	97.4

Table 3. Mechanical properties of Al6061-T6

Modulus of elasticity (GPa)	Maximum tensile strength (MPa)	Yield strength (MPa)	Elongation (%)	Hardness (HB)
68.9	319	276	16.3	107

From these sheets, test specimens measuring 50 mm × 150 mm were prepared using a precision shearing cutter. Before welding, the material underwent a stress-relief heat-treatment process in a reciprocating furnace to stabilise internal stresses and ensure consistent mechanical performance. The heat-treatment schedule, illustrated in Fig 1, involved gradually heating the specimens to 320 °C over one hour, maintaining that temperature for another hour, and then cooling at a controlled rate below 250 °C h^{-1}. This

https://doi.org/10.24191/jmeche.v14i1.8656

procedure was designed to minimise thermal shock and prevent microstructural distortion. The overall process comprised three key phases: a heating stage at 200 °C h^{-1}, a holding stage at 320 °C for uniform temperature distribution, and a controlled cooling stage to ambient temperature.

Tool fabrication details and specifications

The FSW tools were produced from H13 (DIN 1.2344) hot-working steel, known for its high-temperature strength and wear resistance. Their nominal diameter was 25 mm, and the alloy composition is listed in Table 4. Most tool profiles were machined on a Mazak CNC lathe, while the square pins were manufactured using a 1050 CBM CNC milling machine. The tools were subsequently heat-treated by gas carburising at 1030 °C to enhance surface hardness, which was maintained between 45 HRC and 50 HRC.

Table 4. Chemical composition of H13 Steel (wt%)

Cu	0.124
Mo	1.200
Cr	5.230
S	0.009
P	0.021
Mn	0.402
Si	0.955
C	0.353
Fe	90.400

Dimensional details, including shoulder diameter, pin height, and pin-angle configuration, are presented in Table 5. The fixtures used to secure the workpieces during welding were fabricated from St 37 steel. The fixture's top and front-view designs are depicted in Fig 1, showing the four-clamp arrangement that held the aluminium plates in position throughout the FSW process.

Table 5. Tool geometry and dimensions

Tool	Schematic	d_1 (mm)	d_2 (mm)
Conical		Ø3.5	Ø4.5
Threaded cone		Ø3.5	Ø4.5
Cylindrical		Ø3.5	Ø3.5
Square	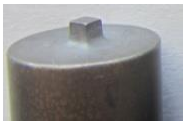	Ø3.5	Ø3.5

https://doi.org/10.24191/jmeche.v14i1.8656

The fabrication of fixtures for holding the workpieces during welding was done using St 37 steel. Fig 1 shows the design of the fixture.

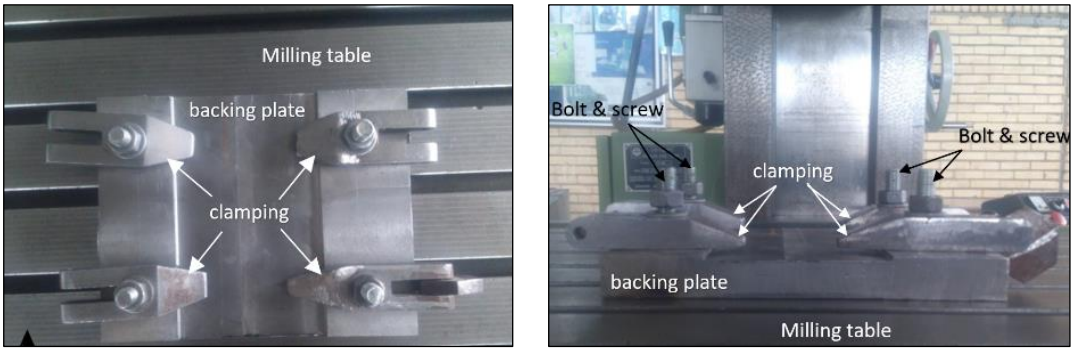

(a) (b)

Fig. 1. (a) The top view of the fixture structure via four clamping mechanisms to the sample specimen in the FSW process, and (b) is the front view.

During the experiment, the conical tool was first aligned on the fixture, and the two aluminium plates were positioned within the fixture groove and tightly fastened with screws. The worktable was then adjusted to align the pin's axis precisely at the joint interface of the sheets. The shoulder was positioned approximately 5 mm to 10 mm from the plate's edge. Welding was performed with the tool rotating counterclockwise. Once the pin made contact, the tool height was carefully adjusted, and the traverse motion was initiated. The operation concluded once the required weld length was reached, after which the tool was withdrawn, and the table lowered. Photographs of the welding setup and completed joints are shown in Fig 2 and Fig 3, respectively.

Force measurement

To record the forces generated during welding, a Kistler B9443 dynamometer was mounted so that its z-axis aligned with the tool axis and its y-axis with the welding direction. This arrangement allowed simultaneous measurement of vertical and traverse forces during the process, as illustrated in Fig 4.

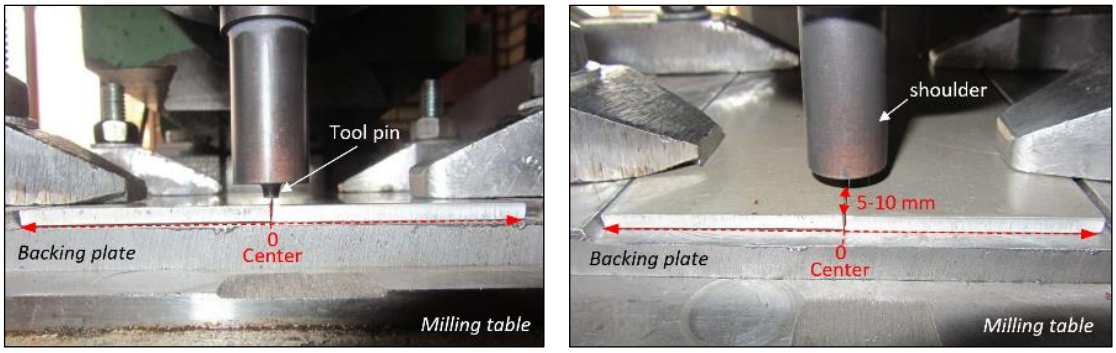

(a) (b)

Fig. 2. (a) Tool pin centering and (b) distance of the tool shoulder from the edge of the sheets.

https://doi.org/10.24191/jmeche.v14i1.8656

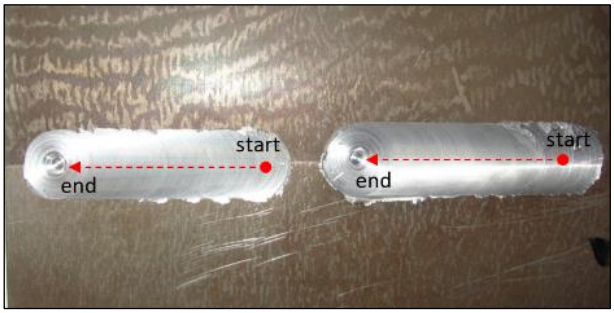

Fig. 3. A completed welding sample.

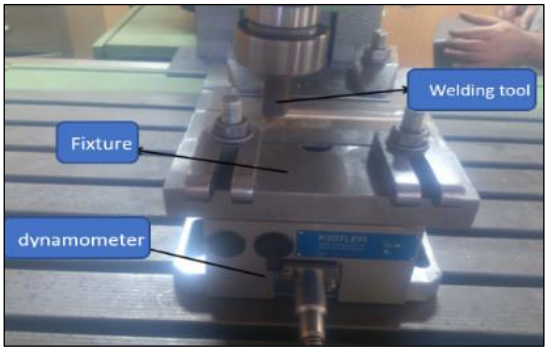

Fig. 4. The place of the dynamometer used for welding.

Tensile test

Following the welding process, the joints were sectioned using a wire-cut machine in accordance with ASTM M8E/8E standards, as illustrated in Fig 5(a). The tensile strength of the specimens was evaluated using a Universal Material Tester (Model 310WP) with a maximum load capacity of 50 kN, operated at a constant cross-head speed of 1 mm·min^{-1} under ambient laboratory conditions, as shown in Fig 5(b).

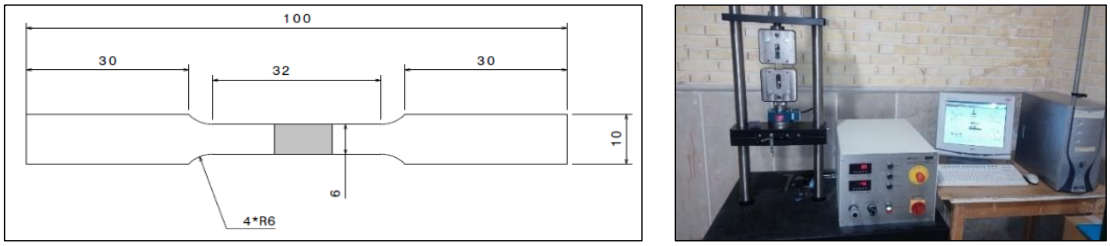

(a) (b)

Fig. 5. (a) Standard dimensions of the tensile sample and (b) the tension device test.

Residual-stress measurement

Residual stresses were evaluated using the hole-drilling technique. A fine hole was machined into each specimen with an Airbin air-driven milling unit (Switzerland) operating at 35,000 rpm and a feed rate of 25 µm min^{-1}. Strain release was recorded through FRS-23-2 strain gauges, and the cutting tool used was a

https://doi.org/10.24191/jmeche.v14i1.8656

six-flute Commet (1.6 mm diameter, Germany). Strain data were captured using a 211TML dynamic strain logger, while hole depth was monitored with a Mitutoyo micrometer of 1 µm accuracy. The general setup for this test is displayed in Fig 6.

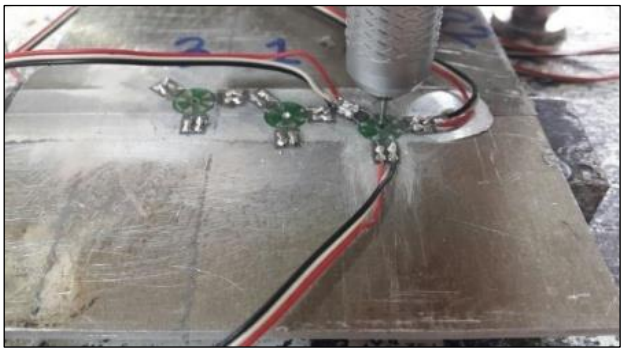

Fig. 6. Central drilling test (for residual stress test).

Experimental design

The overall experimental matrix was created with Minitab software, following a complete factorial design that varied tool tilt angle, feed rate, and rotational speed. Each test condition is listed in Table 6, which specifies the parameter sets used for the 27 samples. Tool-tilt angles of 0°, 2°, and 4° were examined, with corresponding adjustments of feed rate and rotational speed across multiple trials.

Table 6. Experiment design with MiniTab14

Test/ sample number	Rotated-tool speed (rpm)	Feed rate (mm/min)	Tool angle (°)
1	800	40	0
2	800	40	2
3	800	40	4
4	800	80	0
5	800	80	2
6	800	80	4
7	800	125	0
8	800	125	2
9	800	125	4
10	1250	40	0
11	1250	40	2
12	1250	40	4
13	1250	80	0
14	1250	80	2
15	1250	80	4
16	1250	125	0
17	1250	125	2
18	1250	125	4
19	1600	40	0
20	1600	40	2

https://doi.org/10.24191/jmeche.v14i1.8656

21	1600	40	4
22	1600	80	0
23	1600	80	2
24	1600	80	4
25	1600	125	0
26	1600	125	2
27	1600	125	4

RESULTS AND DISCUSSION

Determination of welding parameters

The experimental design incorporated three main factors: rotational speed, feed rate, and tool tilt angle to determine the optimum settings for producing defect-free welds. Each welded specimen was visually and mechanically inspected to verify the quality of the joint and identify any surface irregularities.

Weld defect

During the welding trials, certain parameter combinations resulted in substandard joint integrity. Specifically, specimens numbered 13, 16, and 25 exhibited pronounced surface irregularities and poor weld bead morphology, as shown in Fig 7(a). In contrast, specimen 7 displayed a distinct macrostructural defect in the form of a visible void, rendering it unsuitable for subsequent tensile testing, as illustrated in Fig 7(b).

(a)

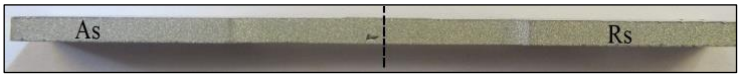

(b)

Fig. 7. (a) Poor surface quality and improper weld appearance and (b) the hole in the weld section for sample 7.

The defects observed in samples welded at a zero-degree tilt angle can be attributed to the reduction of the forging force. When the tool operates without tilt, plasticised material beneath the concave shoulder is not sufficiently compacted into the weld zone, leading to incomplete material consolidation and poor surface finish. This outcome corresponds with prior findings (Armansyah, 2020; Khaki et al., 2019) that emphasizes the necessity of a slight tool tilt for effective forging action.

https://doi.org/10.24191/jmeche.v14i1.8656

In sample 7, produced at a tool speed of 800 rpm, a keyhole defect emerged because of the low heat input associated with the high traverse rate. Insufficient thermal energy restricts material softening and hampers flow around the pin, thereby generating a cavity at the leading edge of the weld, which in turn reduces mechanical strength (Fratini & Zuccarello, 2006).

The formation of internal defects in the weld joint can be attributed to the short interaction time between the tool and the material in the FSW process. At low rotated-tool speeds, the maximum temperature generated during welding is lower, reducing the tool's ability to sufficiently soften and mix the material around the welding pin. Consequently, the material fails to consolidate properly, resulting in internal defects within the weld region (Kubit et al., 2022).

At the opposite extreme, excessively high local temperatures caused by high rotational speed or low feed rate can result in over-plasticisation of material under the shoulder. This condition leads to metal adhesion on the tool and the development of surface pleats or voids, as observed in samples 12, 15, 18, 21, and 24 (Das et al., 2023). These defects stem from unstable material flow and excessive local heat generation that disturb the continuity of the joint.

Tensile strength behaviour

Tensile tests were performed on all welded samples at a constant strain rate of 1 mm min^{-1} using a maximum machine load of 50 kN. The base material exhibited a tensile strength of 253.6 MPa, while the highest value recorded for the welded joints was 211.8 MPa at 1250 rpm, 125 mm min^{-1} feed rate, and a 2° tool tilt as shown in Table 7. These parameters produced the most balanced combination of heat input and material flow, resulting in superior joint consolidation.

Table 7. Fracture stress values of 27 tests/samples numbers

Test/ Sample number	Rotated-tool speed (rpm)	Feed rate (mm/min)	Tool angle (°)	Fracture stress (MPa)
1	800	40	0	174.9
2	800	40	2	180.3
3	800	40	4	191.2
4	800	80	0	188.5
5	800	80	2	185.8
6	800	80	4	177.6
7	800	125	0	105.6
8	800	125	2	206.1
9	800	125	4	197.8
10	1250	40	0	189.8
11	1250	40	2	181.7
12	1250	40	4	181.7
13	1250	80	0	173.2
14	1250	80	2	183.1
15	1250	80	4	191.2
16	1250	125	0	194.7
17	1250	125	2	211.8
18	1250	125	4	203.4
19	1600	40	0	187.1
20	1600	40	2	180.3
21	1600	40	4	179.0

https://doi.org/10.24191/jmeche.v14i1.8656

22	1600	80	0	198.0
23	1600	80	2	189.8
24	1600	80	4	180.3
25	1600	125	0	178.6
26	1600	125	2	191.2
27	125	1600	27	187.1

Effect of feed rate

An increase in feed rate generally reduced the total heat input per unit length, which accelerated cooling and limited the plastic deformation zone. Consequently, weld strength initially improved with rising feed rate but declined when the feed exceeded its optimum value. The trend shown in Fig 8 confirms that moderate feed rates favour strong, fine-grained joints, whereas excessively high rates lead to inadequate mixing and reduced mechanical performance (Fratini & Zuccarello, 2006; Kubit et al., 2022).

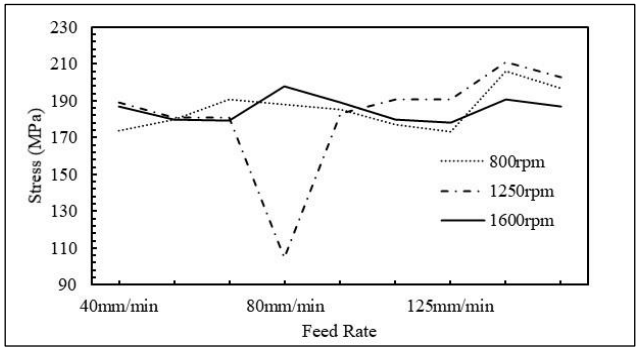

Fig. 8. Changes in fracture stress according to constant rotated-tool speed and variable feed rate.

Effect of rotational speed

Each feed rate corresponded to a specific rotational speed that maximised tensile strength. The relationship between these parameters reflects the trade-off between thermal input and mechanical stirring (Fakkir Mohamed et al., 2021). At lower speeds, incomplete plasticisation leads to weak joints; as the speed increases, the generated heat promotes better bonding until excessive softening causes strength deterioration (Khoshnaw, 2023; Hashmi et al., 2016; Sarnobat et al., 2024). The variation of tensile strength with rotation rate is presented in Fig. 9.

Effect of tool tilt angle

The tool tilt angle exhibited a significant influence on both the forging action and the resultant surface integrity of the welds. A tilt angle of approximately 2° produced optimal results, yielding the highest tensile strength values, as presented in Fig 9(a). Conversely, larger tilt angles caused excessive material stirring and localized thinning, which consequently reduced joint strength, as shown in Fig 9(b). At a 0° tilt angle, the absence of adequate compressive forging led to insufficient material consolidation and the formation of surface discontinuities.

https://doi.org/10.24191/jmeche.v14i1.8656

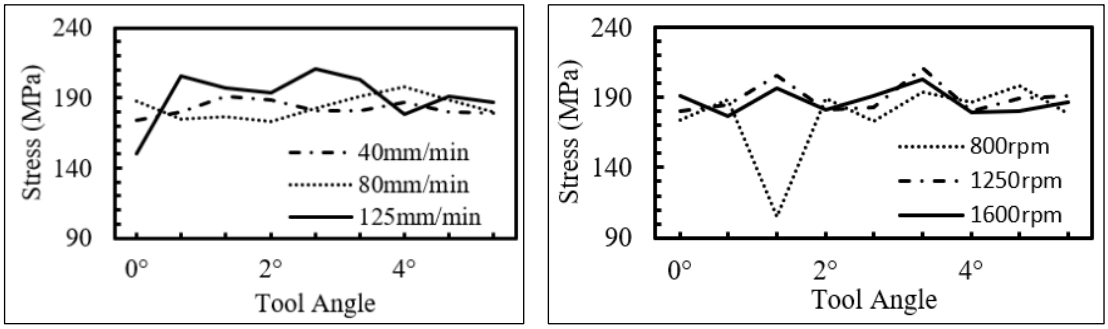

Fig. 9. Effect of tool angle on fracture stress at different (a) feed rate and (b) rotated-tool speed.

Residual stress and weld integrity

To evaluate residual stress and its correlation with mechanical behaviour, tensile and central-drilling tests were carried out on samples welded under optimal parameters. The results show a clear connection between tool geometry and stress distribution. Fig 10 shows that welds produced using the square-pin tool exhibited the highest ultimate tensile strength up to 198.7 MPa. On the other hand, the square-pin tool exhibited the lowest residual stress at 32 MPa, while threaded-conical pins generated the highest residual stress levels up to 95 MPa (refer to Table 8).

Table 8. Strain and stress values

Tool shape	Maximum residual stress (MPa)	Minimum residual stress (MPa)
Conical	49	30
Cylindrical	40	23
Square	32	27
Threaded cone	95	80

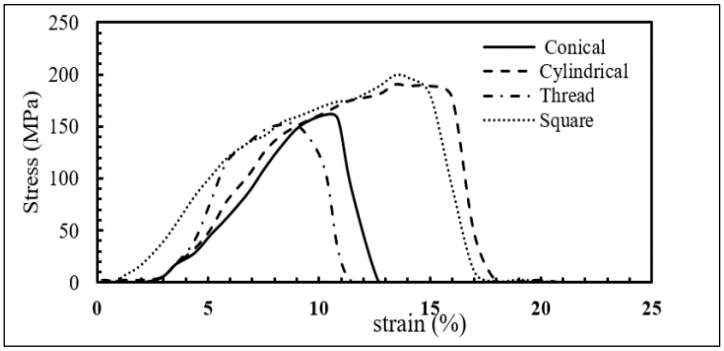

Fig. 10. Charts related to welding tension made with 4 tools.

The superior performance of the square-pin design arises from its ability to impose periodic impact pulses during rotation, which intensifies material mixing and reduces internal voids. Fractography revealed that specimens welded with the square tool fractured outside the weld region, indicating uniform grain distribution and minimal stress concentration. Conversely, welds made using cylindrical and conical tools failed near or within the stir zone due to less effective material flow (refer Fig 11).

https://doi.org/10.24191/jmeche.v14i1.8656

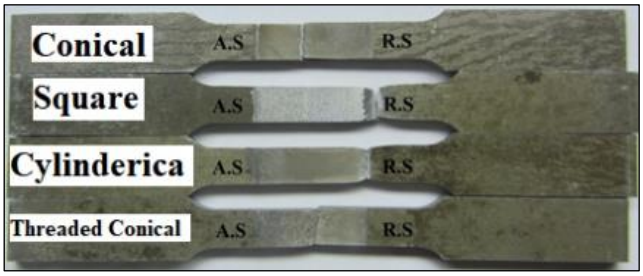

Fig. 11. Fracture location of welded samples.

Dynamometer measurements confirmed that the square tool produced the greatest vertical force with around 3700 N (Fig 12(a)), following the cylindrical-tool with about 1700 N (Fig 12(b)), for conical-tool around 1490 N (Fig 13(a)), and for thread-conical tool about 850 N (Fig 13(b)). The dynamometer measurements confirmation is presented in a bar chart (Fig 14) where the square, cylindrical, conical, and thread-conical tools show their vertical force values of 3700 N, 1700 N, 1490 N, and 850 N, respectively. The higher forging pressure associated with the square tool improved bonding quality, consistent with previous experimental trends (Elangovan & Balasubramanian, 2008b; Khaleel et al., 2023b).

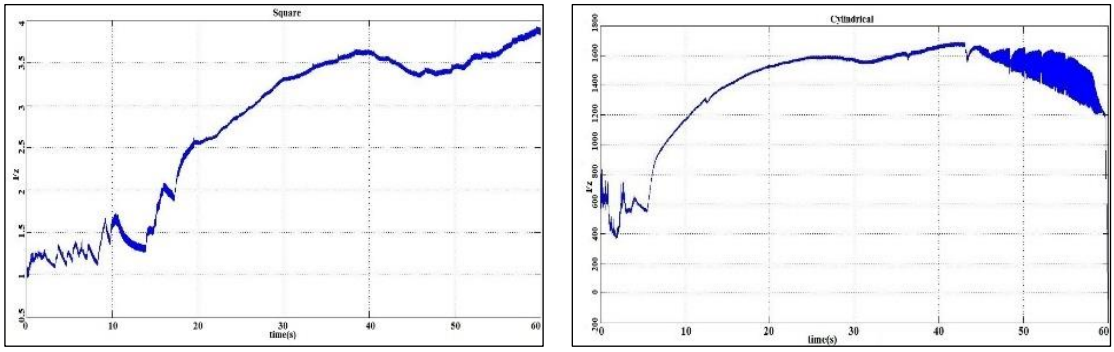

(a) (b)

Fig. 12. Welding force (N) vs. time (sec) for different tool shapes (a) square tool and (b) cylindrical tool.

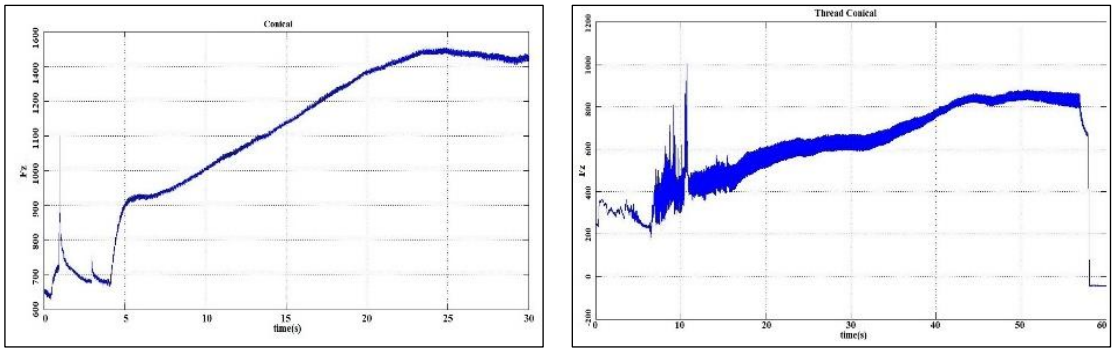

(a) (b)

Fig. 13. Welding force (N) vs. time (sec) for different tool shapes (a) conical tool and (b) threaded conical tool.

https://doi.org/10.24191/jmeche.v14i1.8656

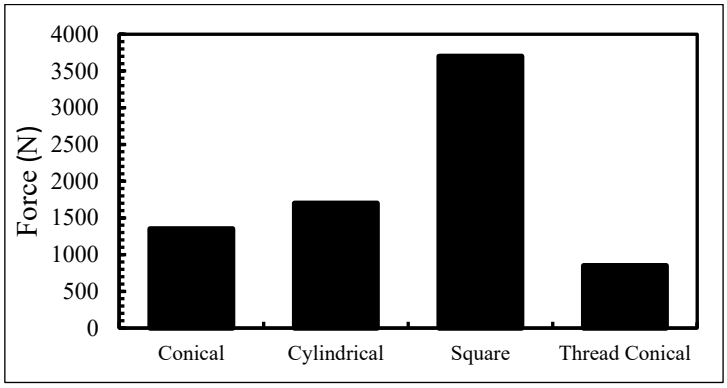

Fig. 14. Maximum welding forces according to the tool shape.

Residual-stress analysis

Residual-stress measurements at various depths revealed that the leading (advancing) side of the weld experienced greater tensile stress than the trailing side, owing to asymmetric heat distribution and material displacement. Data presented in Tables 9 and 10 and visualised in Fig 15 show that stress transitions from compressive near the surface to tensile at deeper regions. Square-pin welds exhibited the most uniform distribution, confirming that effective material compression mitigates residual stress formation.

Table 9. Square tool, rear side

Mininum stress (MPa)	Maximum stress (MPa)	Depth (micron)
-49	-32	100
-24	-1	200
-5	19	300
-1	21	400
6	23	500

Table 10. Square tool, front side

Minimum stress (MPa)	Maximum stress (MPa)	Depth (micron)
-60	-32	100
-27	-1	200
-17	13	300
35	44	400
55	82	500

Validation and reliability of results

Multiple experimental repetitions and cross-validation with literature (Amini et al., 2015; Armansyah et al., 2024; Elangovan & Balasubramanian, 2008b; Khozani et al., 2025; Khaleel et al., 2023c; Kolahdooz, 2018; Khaki et al., 2019) confirmed the reproducibility and accuracy of the results. All equipment was calibrated prior to testing to maintain measurement precision. Statistical analysis indicated consistent trends in tensile strength, stress variation, and fracture mode, demonstrating the robustness of the findings. Visual and mechanical inspections of failure zones further validated the reliability of the experimental conclusions.

https://doi.org/10.24191/jmeche.v14i1.8656

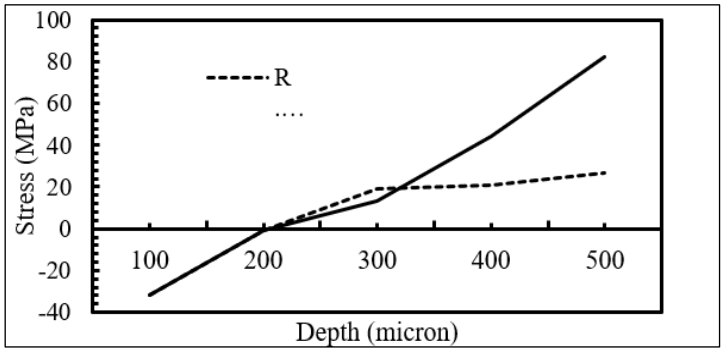

Fig. 15. Comparing the amount of stress on the front (A.S) and rear (R.S) side.

CONCLUSION

This research systematically examined how tool geometry, rotational speed, feed rate, and tilt angle influence the mechanical behaviour and residual stress of friction stir welded aluminium alloy 6061-T6. The analysis identified the optimal parameters as a rotational speed of 1250 rpm, a feed rate of 125 mm min^{-1}, and a tool tilt of 2°. Under these settings, the welds exhibited an ultimate tensile strength of approximately 211.9 MPa, equivalent to about 87% of the base material's strength. The results demonstrated that insufficient tilt (0°) reduces the forging action, leading to surface discontinuities, while excessive tilt (4°) causes over-stirring and local thinning that compromise strength. For constant rotational speed, tensile strength initially increases with feed rate due to more efficient heat control, but decreases beyond the optimum. Similarly, at a constant feed rate, raising tool speed improves bonding up to a threshold, beyond which excessive thermal input softens the material and weakens the joint. Among the four pin geometries evaluated, the square tool consistently delivered the highest tensile strength and the lowest residual stress, attributed to its stronger mechanical agitation and enhanced material consolidation during welding. Dynamometer data confirmed that this tool shape generated the greatest vertical force, which helped compact the plasticised material and prevent voids. The observed correlation between increased weld strength and reduced residual stress indicates that proper parameter selection can simultaneously improve structural performance and minimize distortion. Overall, the findings establish a reliable process window for friction stir welding of aluminium 6061-T6. They provide a practical foundation for industrial optimization and future studies integrating microstructural analysis such as scanning electron microscopy (SEM) to further clarify how tool geometry and heat generation govern local deformation and grain refinement.

ACKNOWLEDGMENT

The authors express sincere appreciation to Universitas Pembangunan Nasional Veteran Jakarta, Indonesia, BEHnam Pajouh Sepahan Industrial, Iran, Aerospace Systems Research Center, Gyeongsang National University, Republic of Korea, and the Faculty of Technology, De Montfort University, United Kingdom, for their invaluable technical collaboration and institutional support throughout this study.

https://doi.org/10.24191/jmeche.v14i1.8656

FUNDING

This work was supported by the "HIBAH PENELITIAN NON-SERDOS 2023" [128.1/UN.61.0/HK.07/LIT.DBD.S3/2023].

CONFLICT OF INTERESTS

The authors agree that this research was conducted in the absence of any self-benefits, commercial or financial conflicts, and declare the absence of conflicting interests with the funders.

CONTRIBUTIONS OF AUTHORS

The authors confirm the equal contribution in each part of this work. All authors reviewed and approved the final version of this work.

REFERENCES

Amini, S., Amiri, M. R., & Barani, A. (2015). Investigation of the effect of tool geometry on friction stir welding of 5083-O aluminum alloy. The International Journal of Advanced Manufacturing Technology, 76(1–4), 255–261. https://doi.org/10.1007/s00170-014-6277-6

Armansyah (2020). Friction stir spot welded characterization of aluminium alloy 5052-H112 and prediction model using Artificial Neural Network [Doctoral thesis, Universiti Teknologi MARA]. Retrieved from https://ir.uitm.edu.my/id/eprint/32514/

Armansyah, Chie, H. H., Saedon, J., & Adenan, S. (2020). Feed-forward back-propagation (FFBP) algorithm for property prediction in friction stir spot welding of aluminium alloy. IOP Conference Series: Earth and Environmental Science, 426, 012128. https://doi.org/10.1088/1755-1315/426/1/012128

Armansyah, Kuncoro, C. B. D., Wiguna, R., Firmansyah, R., & Rianto, R. B. (2024). Tensional shear load characterization of pin-less friction stir spot welding on aluminium 1100-H12 based on varied parameters. AIP Conference Proceedings, 3115, 040002. https://doi.org/10.1063/5.0207276

Bahrami, M., Besharati Givi, M. K., Dehghani, K., & Parvin, N. (2014). On the role of pin geometry in microstructure and mechanical properties of AA7075/SiC nano-composite fabricated by friction stir welding technique. Materials & Design, 53, 519–527. https://doi.org/10.1016/j.matdes.2013.07.049

Baiyao, H., Hua, Z., & Fuad, K. (2020). Mechanical behavior associated with metallurgical aspects of friction stir welded Al–Li alloy exposed to exfoliation corrosion test. Materials Research Express, 7(6), 066502. https://doi.org/10.1088/2053-1591/ab95d7

Buglioni, L., Tufaro, L. N., & Svoboda, H. G. (2015). Thermal cycles and residual stresses in FSW of aluminum alloys: experimental measurements and numerical models. Procedia Materials Science, 9, 87–96. https://doi.org/10.1016/j.mspro.2015.04.011

Das, D., Bag, S., Pal, S., & Sharma, A. (2023). Material defects in friction stir welding through thermo–mechanical simulation: dissimilar materials with tool wear consideration. Materials, 16(1), 301.

https://doi.org/10.3390/ma16010301

Elangovan, K., & Balasubramanian, V. (2008a). Influences of tool pin profile and tool shoulder diameter on the formation of friction stir processing zone in AA6061 aluminium alloy. Materials & Design, 29(2), 362–373. https://doi.org/10.1016/j.matdes.2007.01.030

Elangovan, K., & Balasubramanian, V. (2008b). Influences of tool pin profile and welding speed on the formation of friction stir processing zone in AA2219 aluminium alloy. Journal of Materials Processing Technology, 200(1–3), 163–175. https://doi.org/10.1016/j.jmatprotec.2007.09.019

El-Rayes, M. M., & El-Danaf, E. A. (2012). The influence of multi-pass friction stir processing on the microstructural and mechanical properties of Aluminum Alloy 6082. Journal of Materials Processing Technology, 212(5), 1157–1168. https://doi.org/10.1016/j.jmatprotec.2011.12.017

Fakkir Mohamed, M., Yaknesh, S., Anantha Kumar, C. M., Godwin Rajadurai, J., Janarthanan, S., & Vignes, A. V. S. (2021). Optimization of friction stir welding parameters for enhancing welded joints strength using Taguchi based grey relational analysis. Materials Today: Proceedings, 39(1), 676–681. https://doi.org/10.1016/j.matpr.2020.09.188

Fratini, L., & Zuccarello, B. (2006). An analysis of through-thickness residual stresses in aluminium FSW butt joints. International Journal of Machine Tools and Manufacture, 46(6), 611–619. https://doi.org/10.1016/j.ijmachtools.2005.07.013

Hashmi, K. H., Zakria, G., Raza, M. B., & Khalil, S. (2016). Optimization of process parameters for high speed machining of Ti-6Al-4V using response surface methodology. The International Journal of Advanced Manufacturing Technology, 85(5–8), 1847–1856. https://doi.org/10.1007/s00170-015-8057-3

Hutchings, M. T., Withers, P. J., Holden, T. M., & Lorentzen, T. (2005). Introduction to the characterization of residual stress by neutron diffraction. (1st Ed.). CRC Press.

Ilangovan, M., Rajendra Boopathy, S., & Balasubramanian, V. (2015). Effect of tool pin profile on microstructure and tensile properties of friction stir welded dissimilar AA 6061–AA 5086 aluminium alloy joints. Defence Technology, 11(2), 174–184. https://doi.org/10.1016/j.dt.2015.01.004

Khaki, S., Heidari, A., & Kolahdooz, A. (2019). Optimizing friction stir welding process for enhancing strength and hardness using Taguchi multi-objective function method. International Journal of Advanced Design and Manufacturing Technology, 12(3), 25-33.

Khaleel, H. H., Mahmood, I. A., & Khoshnaw, F. (2023a). Fatigue and impact properties of single and double resistance spot welding for high-strength steel used in automotive applications. Journal of the Brazilian Society of Mechanical Sciences and Engineering, 45(3), 155. https://doi.org/10.1007/s40430-023-04080-6

Khaleel, H. H., Mahmood, I. A., & Khoshnaw, F. (2023b). Optimization process of double spots welding of high strength steel using in the automotive industry. Engineering and Technology Journal, 41(1), 110–120. https://doi.org/10.30684/etj.2022.134325.1236

Khaleel, H. H., Mahmood, I. A., & Khoshnaw, F. (2023c). Analysis of double resistance spot welding's failure in high strength low alloy steel. Journal of Applied Engineering Science, 21(2), 547–560. https://doi.org/10.5937/jaes0-40923

Khoshnaw, F. (2023). Welding of metallic materials. Methods, metallurgy, and performance. Elsevier.

Khozani, A. K., Alavi, S. A., Afshari, M., Afshari, H., Al-hedrewy, M., Samadi, M. R., & Beygi, R. (2025).

An enhancement of the yield strength and hardness in the friction stir welding of AZ31/AA3105 joint. Journal of Adhesion Science and Technology, 39(3), 345–372. https://doi.org/10.1080/01694243.2024.2403687

Kolahdooz, A. (2018). Investigation of the hardness improvement for Al-A380 alloy using the controlled atmosphere in the mechanical stirring casting method. Proceedings of the Institution of Mechanical Engineers, Part E: Journal of Process Mechanical Engineering, 233(2), 225–233. https://doi.org/10.1177/0954408918773526

Kolahdooz, A., Nourouzi, S., Bakhshi, M., & Hosseinipour, S. J. (2014). Investigation of the controlled atmosphere of semisolid metal processing of A356 aluminium alloy. Journal of Mechanical Science and Technology, 28(10), 4267–4274. https://doi.org/10.1007/s12206-014-0940-6

Kubit, A., Trzepieciński, T., Kluz, R., Ochałek, K., & Slota, J. (2022). Multi-criteria optimisation of friction stir welding parameters for EN AW-2024-T3 aluminium alloy joints. Materials, 15(15), 5428. https://doi.org/10.3390/ma15155428

Maneiah, D., Mishra, D., Rao, K. P., & Raju, K. B. (2020). Process parameters optimization of friction stir welding for optimum tensile strength in Al 6061-T6 alloy butt welded joints. Materials Today: Proceedings, 27(2), 904–908. https://doi.org/10.1016/j.matpr.2020.01.215

Moghadam, D. G., Doost, K. F., Mohammadabadi, A. R., & Moghadam, M. R. (2015). Tool's speed effect on hardness and residual stress in friction stir welded Al 2024-T351: experimental method and numerical simulation. Journal of Modares Mechanical Engineering, 15(2), 61–71. https://dor.isc.ac/dor/20.1001.1.10275940.1394.15.2.18.6

Newishy, M., Jaskari, M., Järvenpää, A., Fujii, H., & Abdel-Aleem, H. A. (2023). Friction stir welding of dissimilar Al 6061-T6 to AISI 316 stainless steel: microstructure and mechanical properties. Materials, 16(11), 4085. https://doi.org/10.3390/ma16114085

Reza-E-Rabby, M., & Reynolds, A. P. (2014). Effect of tool pin thread forms on friction stir weldability of different aluminum alloys. Procedia Engineering, 90, 637–642. https://doi.org/10.1016/j.proeng.2014.11.784

Richter-Trummer, V., Suzano, E., Beltrão, M., Roos, A., dos Santos, J. F., & de Castro, P. M. S. T. (2012). Influence of the FSW clamping force on the final distortion and residual stress field. Materials Science and Engineering: A, 538, 81–88. https://doi.org/10.1016/j.msea.2012.01.016

Rossini, N. S., Dassisti, M., Benyounis, K. Y., & Olabi, A. G. (2012). Methods of measuring residual stresses in components. Materials & Design, 35, 572–588. https://doi.org/10.1016/j.matdes.2011.08.022

Sadeghi, S., Najafabadi, M. A., Javadi, Y., & Mohammadisefat, M. (2013). Using ultrasonic waves and finite element method to evaluate through-thickness residual stresses distribution in the friction stir welding of aluminum plates. Materials & Design (1980-2015), 52, 870–880. https://doi.org/10.1016/j.matdes.2013.06.032

Sarnobat, S., Kumar, I., Saxena, K. K., & Malik, V. (2024). Investigation on the mechanical properties and microstructural analysis of dissimilar friction stir welding of AA5154/AA7150. Journal of Adhesion Science and Technology, 38(21), 4010–4036. https://doi.org/10.1080/01694243.2024.2362029

https://doi.org/10.24191/jmeche.v14i1.8656